Synthesis and Anti-Pancreatic Cancer Activity Studies of Novel 3-Amino-2-hydroxybenzofused 2-Phospha-γ-lactones

Satheesh Krishna Balam, Jayaprakash Soora Harinath, Suresh Kumar Krishnammagari, Raghavendra Reddy Gajjala, Kishore Polireddy, Vijaya Bhaskar Baki, Wei Gu, Koteswara Rao Valasani, Vijaya Kumar Reddy Avula, Swetha Vallela, Grigory Vasilievich Zyryanov, Visweswara Rao Pasupuleti,* and Suresh Reddy Cirandur*
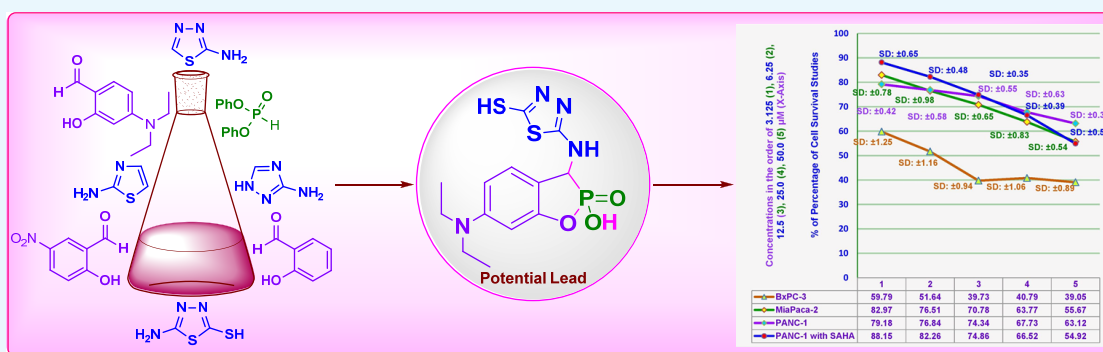
ACCESS | Metrics & More | Article Recommendations | Supporting Information

ABSTRACT: A series of 3-amino-2-hydroxybenzofused 2-phosphalactones (**4a−l**) has been synthesized from the Kabachnik−Fields reaction *via* a facile route from a one-pot three-component reaction of diphenylphosphite with various 2-hydroxybenzaldehyes and heterocyclic amines in a new way of expansion. The *in vitro* anti-cell proliferation studies by MTT assay have revealed them as potential Panc-1, Miapaca-2, and BxPC-3 pancreatic cell growth inhibitors, and the same is supported by molecular docking, QSAR, and ADMET studies. The MTT assay of their SAHA derivatives against the same cell lines evidenced them as potential HDAC inhibitors and identified **4a**, **4b**, and **4k** substituted with 1,3-thiazol, 1,3,4-thiadiazol, and 5-sulfanyl-1,3,4-thiadiazol moieties on phenyl and diethylamino phenyl rings as potential ones. Additionally, the flow cytometric analyses of **4a**, **4b**, and **4k** against BxPC-3 cells revealed compound **4k** as a lead compound that arrests the *S* phase cell cycle growth at low micromolar concentrations. The ADMET properties have ascertained their inherent pharmacokinetic potentiality, and the wholesome results prompted us to report it as the first study on anti-pancreatic cancer activity of cyclic α-aminophosphonates. Ultimately, this study serves as a good contribution to update the existing knowledge on the anticancer organophosphorus heterocyclic compounds and elevates the scope for generation of new anticancer drugs. Further, the studies like QSAR, drug properties, toxicity risks, and bioactivity scores predicted for them have ascertained the synthesized compounds as newer and potential drug candidates. Hence, this study had augmented the array of α-aminophosphonates by adding a new collection of 3-amino-2-hydroxybenzofused 2-phosphalactones, a class of cyclic α-aminophosphonates, to it, which proved them as potential anti-pancreatic cancer agents.

■ INTRODUCTION

Organophosphorus chemistry has offered many catalysts for the successful accomplishments of complex[1] and coupling[2] reactions by the action of potential catalyst promoters.[3] In medicinal perspectives, some of them have been identified as potential antioxidant,[4] antifungal,[5] antibacterial,[6−8] antidiabetic,[9] anticancer,[10] antithrombotic,[11] and antimicrobial[12] agents. Their re-emergence in the field of medicinal chemistry made it amplified as many of them were impregnated with potential moieties in its design itself[13] and identified with a wide array of applications.[14] α-Aminophosphoryl functionality on a pharmacophoric core promotes antitumor activity[15] and

strongly inhibits the human tumor growth and induces apoptosis *via* the mitochondria-dependent pathway[16] on safe and non-toxic grounds without affecting the normal cells.[17] The recent reports on the biological activity evaluation studies of organophosphorus heterocycles reveal that this is a search
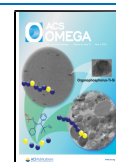
thrust area with perpetual contributions.[18] Such inherent anticancer potentiality of α-aminophosphonates[19−25] has inspired us to design and synthesize some new 3-amino functionalized benzofused phospha-γ-lactones with a potential core of the 2,5-dihydro-1,2-oxaphosphole-2-oxide moiety[26] and investigate their pancreatic cell inhibition activity. Meanwhile, the previous methodologies for the synthesis of benzofused 2-phospha-γ-lactones involves the utility of precursors like aldols,[27] divinyl ethers,[26] acetylene carboxylic acids,[26] chalcones,[26] allenes,[28,29] and alkynyl systems[30−34] along with phosphorylating agents like dichlorophenylphosphines,[32,35,36] dichlorophenyl phosphineoxides,[37] triphenyl phosphine,[31,34] trialkylphosphite,[38] 3-methylbuta-1,2-dien-1-ylphosphonic dichlorides,[39] allenyl phosphonates,[40] and dialkyl phosphites.[33,41] The present route for the synthesis of 2,5-dihydro-1,2-oxaphosphole-2-oxide core is highly adaptable with simple reaction procedures and hence eliminates the use of expensive precursors (Figure 1).

As phospha-coumaranones (phospha-γ-lactones) are analogues of coumaranones (coumaran derivatives) by structure and as coumaranones are potential antiplasmodial,[42] antifungal,[43] anti-neoplasia,[44] and anticancer[45] agents, we have designed the synthesis of their phosphorus analogues bearing a cyclic phosphonic acid group (hydroxy group located on the phosphoryl group), which easily facilitates ring opening operations in vivo metabolic processes (hydrolysis) and hence acts as potential prodrugs.[46] This has motivated us to investigate the anti-pancreatic cancer activity and to identify the mechanistic aspects of cell cycle inhibition. Ultimately, authors have synthesized the title compounds and reported **4k** with 5-sulfanyl-1,3,4-thiadiazolyl, and diethylamino phenyl rings interlinked by an aminophosphoryl moiety is identified as potential inhibitors against S (synthesis) phase cell cycle inhibition as ascertained by flow cytometry studies at low micromolar concentrations. The literature study reveals that this is the first contribution on the anti-pancreatic cancer activity of phospha-γ-lactones having a cyclic aminophosponate moiety.

■ RESULTS AND DISCUSSION

Chemistry. The synthesis of novel 3-amino-substituted benzofused 2-phospha-γ-lactones derivatives (**4a−l**) with a core of 3-heteroarylamino-substituted-1,2-oxaphopholicacids has been accomplished by a facile one-pot three-component reaction of various 2-hydroxybenzaldehyes, heterocyclic amines, and diphenyl phosphite (Scheme 1). The regular mechanistic approach of the Kabachnik−Fields reaction for the synthesis of α-aminophosphonate (**I**) from aldehyde, amine, and phosphite has been expanded as such its aryloxy oxygen internally attacks on phosphoryl phosphorus and forms the phospha-γ-lactone monoester (**II**) at elevated temperatures. In the next step, the liberated water of the reaction hydrolyzes the monoester (**II**) at the same elevated temperatures and ultimately forms the phospha-γ-lactone (**III**) as designed and as shown in the plausible mechanism (Figure 2). It is observed that the conversion of **II** to **III** was successful simply with the prolonged heating and does not need any external reagent and catalyst. Hence, this one-pot three-component single-step methodology has been identified as a cost-effective and step-economic reaction to offer phospha-γ-lactones in short reaction times.

The key mechanistic facet directing the design and synthesis of 2-hydroxy phospha-γ-lactones is the presence of the o-
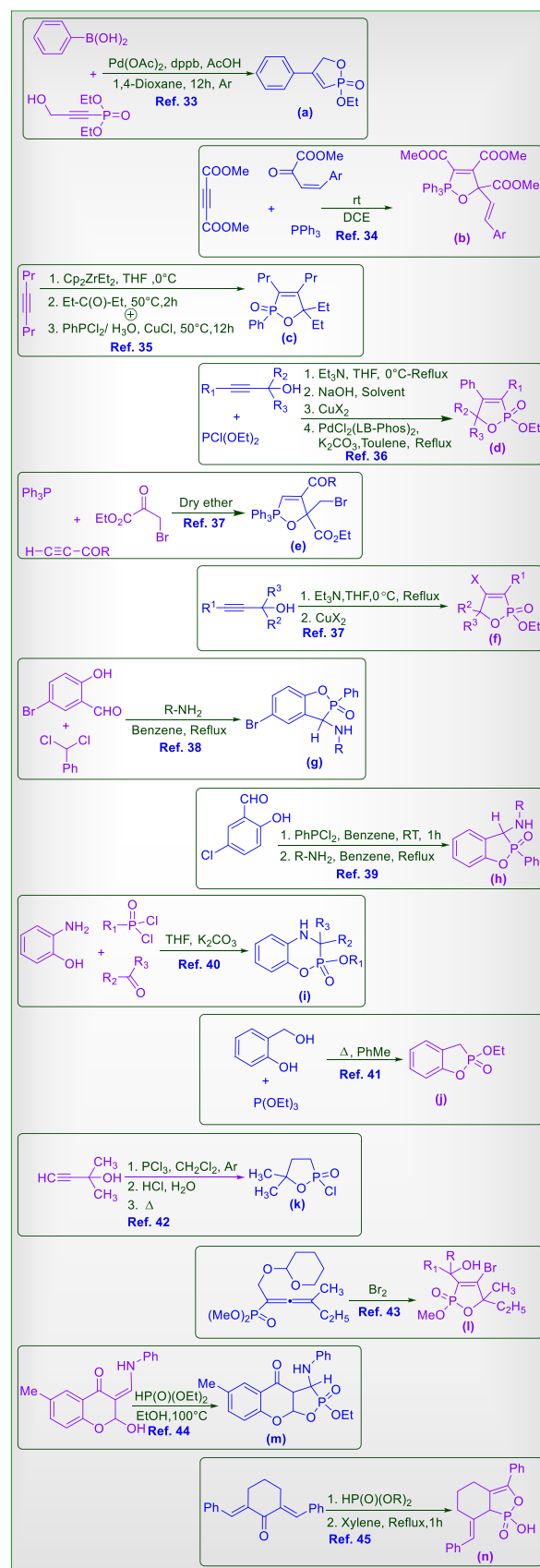

Figure 1. Methods for the synthesis of phospha-γ-lactones.

hydroxy group on aryl aldehyde and re-consumption of the liberated water into the reaction. The scope of the formation of

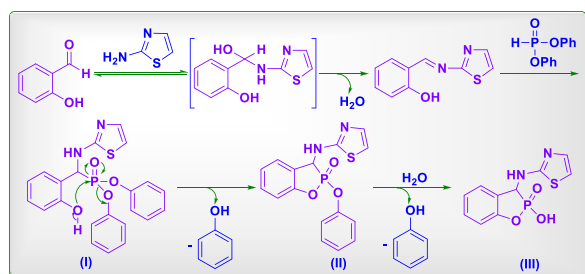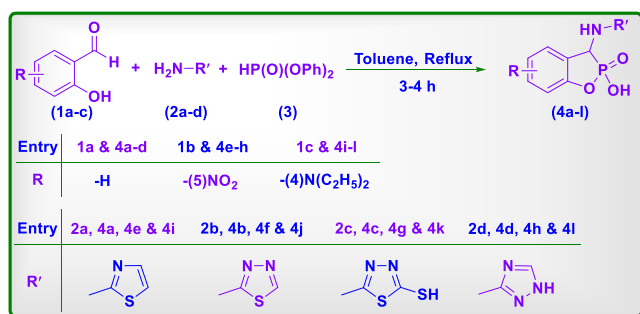**Scheme 1. Synthesis of 3-Amino-Substituted Benzofused Phosphalactone Derivatives**

Figure 2. Mechanism for the synthesis of phospha-γ-lactones.

phospha-γ-lactones from the expansion of Kabachnik−Fields reaction has been investigated with various phosphites like dimethylphosphite, diethylphosphite, *di-i*-propylphosphite, dibutylphosphite, *di-t*-butylphosphite, and dibenzylphosphite along with diphenylphosphite under same reaction conditions. However, none of them have resulted a phospha-γ-lactone monoester or its acid except diphenylphosphite, which is a product-specific reaction with respect to diphenylphosphite (Figure 3).
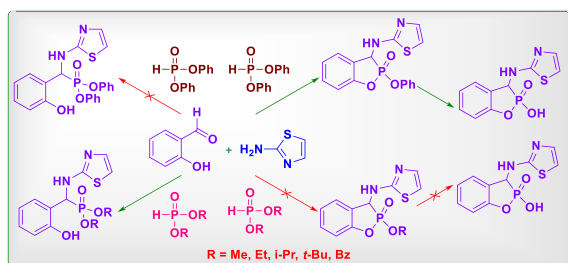

Figure 3. Scope of expansion of the Kabachnik−Fields reaction.

In productivity point, nitro-substituted salicylaldehyde has offered high product yields when compared to diethylamino-substituted salicylaldehyde and unsubstituted salicylaldehyde. Similarly, the reactivity of amines has also followed an order that thiazol-2-amine had offered the high product yields and 1,3,4-thiadiazol-2-amine, 1*H*-1,2,4-triazol-3-amine, and 5-amino-1,3,4- thiadiazole-2-thiol are aligned in the sequence of decreasing product yields. Studies in varying salicylaldehydes and amines are currently under study for further exploration of their synthetic utility in order to evaluate their anti-cell proliferation activities against other cancer cell lines.

The chemical structures of **4a−l** were established by IR, ^{1}H, ^{13}C, and ^{31}P NMR spectral and mass spectrometric studies and elemental analyses. IR absorptions were observed at 3433−

3416, 1238−1222, and 1096−1076 cm^{-1} for NH, P═O, and P−O stretching vibrations.[47,48] Two ^{1}H NMR singlet characteristic peaks for −NH−C$\underline{H}$− (C-3) proton at δ 3.98−3.93 and for −N$\underline{H}$−CH− (C-10) proton at δ 4.28−4.24 were observed.[48,49] The ^{13}C characteristic peak for P−C$\underline{H}$ (C-3) carbon was observed at δ 74.6−63.2.[48,49] The ^{31}P characteristic peaks were observed as singlet at δ 19.58−16.36 for P═O.[48] The mass spectra of **4a−l** confirmed significant molecular and daughter ion peaks at expected m/z values.

Cytotoxicity Assay. Compounds **4a−l** were screened *in vitro* for pancreatic cancer cell inhibition assay on BxPC-3 (Table 1), Miapaca-2 (Table 2), Panc-1 (Table 3), and Panc-1 with SAHA (suberoyl + anilide + hydroxamic acid) bound (Table 4) cell lines, and the results are presented in Tables 1−4, respectively. The anticancer activity of **4a−l** and their SAHA-treated models were assessed by MTT assay with increasing concentrations. Treating of BxPC-3 cells with **4a−l** revealed that **4a**, **4b**, and **4k** have arrested the cell proliferation dose dependently and are identified as potential inhibitors at 50 μM/L (maximum effective concentration) and inhibited the BxPC-3 cell growth to greater than 50%. The % of cell survival profiles of compound **4k** (BxPC-3, Miapaca-2, and Panc-1) and its SAHA derivative (Panc-1 cells) is presented in Figure 4. The results of cytotoxicity assay have provided a rationale for further studies on HDAC inhibition and other human pancreatic malignancies *viz.*, Panc-1, Miapaca-2, and BxPC-3, and hence we have performed the cell cycle analysis for the potential compounds **4a**, **4b**, and **4k**.

S Phase Cell Cycle Arrest. In understanding the mode of the mechanism by which compounds **4a**, **4b**, and **4k** are regulating the growth and proliferating the BxPC-3 cells, we have performed the flow cytometric cell cycle analysis on treated BxPC-3 cells and identified that the treatment of **4k** resulted in an increased percentage of cells in the *S* phase of the cell cycle compared to DMSO control [**4k** (G_0/G_1 phase: 45.5 ± 0.6; *S* phase: 27.2 ± 0.7; G_2/M phase: 26.7 ± 0.2) and DMSO control (G_0/G_1 phase: 69.70 ± 0.6; *S* phase: 13.0 ± 0.2; G_2/M phase: 16.9 ± 0.4)] (Figure 5). This has suggested that **4k** suppresses the BxPC-3 cell cycle progress into next phases by regulating the *S* phase, where compounds **4a** and **4b** are identified as comparatively less significant and identified **4k** as a potential lead compound.

Molecular Docking Studies. Molecular docking properties of **4a−l** have evolved from the selective protein of the pharmacological target regulating the cell proliferation of the pancreatic cancer cell lines. The H-bond interactions of **4a−l** with cancer therapeutic targets formed among H-bond acceptors and donors (Acc and Don), H-bond acceptors (Acc), and aromatic centers (Aro) in the substructure of the tryptophan moiety and phosphate moiety against the arene−cation and arene−arene interactions against the functional groups located on the residues of the inhibitor binding sites, sustaining the downregulation of signaling of the cancer cell by profoundly inhibiting and inactivating the target protein, which is a vital task. The two-dimensional ligand−receptor interaction representation maps are shown in Figure 6.

The ligand data was predicted for the novel ligands (molecules) bound to the proteins that were docked at the target-specified binding domains of the 3HNC receptor. Cumulatively, more than 30 conformations were captured for each ligand−receptor complex pair. Among these binding conformations, the confirmation with the least docking score was taken into account of the study. Where the identified

Table 1. Percentage of BxPC-3 Cell Survival Studies

entry	concentrations					IC$_{50}$ (μg/mL)
	3.125 μM	6.25 μM	12.5 μM	25.0 μM	50.0 μM	
4a	71.88 ± 0.36	64.91 ± 0.57	54.35 ± 0.69	48.32 ± 0.82	37.99 ± 1.13	27.72
4b	77.27 ± 0.16	69.30 ± 0.34	60.34 ± 0.51	56.46 ± 0.79	45.98 ± 0.93	39.64
4c	80.54 ± 1.17	73.49 ± 0.62	68.44 ± 0.54	62.75 ± 0.33	57.78 ± 1.14	62.97
4d	90.32 ± 0.84	81.26 ± 0.38	77.42 ± 0.49	65.28 ± 0.51	52.36 ± 0.84	53.90
4e	95.03 ± 1.07	89.11 ± 0.80	85.63 ± 0.91	82.61 ± 0.75	71.22 ± 0.21	96.40
4f	95.25 ± 0.23	87.63 ± 0.35	78.17 ± 0.48	69.28 ± 0.19	60.49 ± 0.38	60.62
4g	96.73 ± 0.24	91.71 ± 0.12	87.56 ± 0.54	79.95 ± 0.39	72.53 ± 0.69	92.83
4h	98.54 ± 0.58	99.48 ± 0.17	93.72 ± 0.42	92.70 ± 0.81	84.22 ± 0.73	159.55
4i	93.28 ± 0.77	88.45 ± 0.82	79.66 ± 0.52	68.14 ± 0.89	59.79 ± 0.27	59.46
4j	97.62 ± 0.59	86.40 ± 0.45	78.23 ± 0.19	66.38 ± 1.10	56.38 ± 0.86	53.25
4k	59.79 ± 1.25	51.64 ± 1.16	39.73 ± 0.94	40.79 ± 1.06	39.05 ± 0.89	8.48
4l	91.22 ± 0.95	85.36 ± 0.76	76.54 ± 0.83	61.22 ± 0.61	55.67 ± 0.87	51.68

Table 2. Percentage of MiaPaca-2 Cell Survival Studies

entry	concentrations					IC$_{50}$ (μg/mL)
	3.125 μM	6.25 μM	12.5 μM	25.0 μM	50.0 μM	
4a	85.63 ± 1.28	79.40 ± 0.96	72.33 ± 0.89	61.44 ± 0.37	51.42 ± 0.49	48.19
4b	81.37 ± 1.02	77.61 ± 0.88	70.45 ± 0.24	63.65 ± 0.72	53.27 ± 0.56	52.83
4c	91.54 ± 0.87	87.69 ± 0.85	77.18 ± 0.67	64.60 ± 0.57	59.37 ± 0.78	57.74
4d	92.38 ± 0.76	85.75 ± 0.84	73.58 ± 0.62	65.64 ± 0.45	60.82 ± 0.52	60.74
4e	94.63 ± 0.77	86.22 ± 0.86	79.59 ± 0.75	73.30 ± 0.68	66.29 ± 0.58	75.70
4f	97.72 ± 0.76	91.53 ± 0.88	86.66 ± 0.45	81.36 ± 0.36	75.43 ± 0.39	105.37
4g	96.15 ± 1.26	93.39 ± 0.99	89.15 ± 0.87	83.06 ± 0.65	80.47 ± 0.71	138.35
4h	93.19 ± 0.43	91.11 ± 0.68	88.09 ± 0.72	82.84 ± 0.57	79.78 ± 0.31	151.61
4i	94.72 ± 0.77	86.65 ± 0.85	79.47 ± 0.96	72.54 ± 0.63	65.42 ± 0.72	72.68
4j	95.61 ± 1.32	88.29 ± 1.09	82.54 ± 0.26	77.54 ± 0.78	71.65 ± 0.53	93.48
4k	82.97 ± 0.78	76.51 ± 0.98	70.78 ± 0.65	63.77 ± 0.83	55.67 ± 0.54	56.73
4l	99.76 ± 0.98	92.35 ± 0.54	86.54 ± 0.49	81.78 ± 0.67	74.32 ± 0.59	96.95

Table 3. Percentage of PANC-1 Cell Survival Studies

entry	concentrations					IC$_{50}$ (μg/mL)
	3.125 μM	6.25 μM	12.5 μM	25.0 μM	50.0 μM	
4a	90.99 ± 0.96	86.24 ± 0.82	75.58 ± 0.54	67.54 ± 0.66	61.04 ± 0.90	62.72
4b	94.27 ± 0.67	88.03 ± 0.94	78.73 ± 1.14	66.95 ± 0.81	62.49 ± 0.75	62.89
4c	97.51 ± 0.92	89.65 ± 0.87	82.84 ± 0.76	76.98 ± 0.85	73.43 ± 0.69	95.68
4d	98.67 ± 0.72	96.14 ± 0.69	91.36 ± 0.44	89.76 ± 0.58	84.11 ± 0.85	167.34
4e	99.45 ± 0.25	98.65 ± 0.37	96.88 ± 0.36	92.13 ± 0.42	87.99 ± 0.53	199.09
4f	95.08 ± 0.76	92.45 ± 0.64	90.43 ± 0.78	88.67 ± 0.28	84.37 ± 0.87	215.66
4g	99.07 ± 0.62	95.92 ± 0.54	89.84 ± 0.48	87.07 ± 0.32	84.90 ± 0.45	170.87
4h	99.48 ± 0.54	97.56 ± 0.65	94.39 ± 0.49	91.50 ± 0.37	87.04 ± 0.53	194.23
4i	94.15 ± 0.77	90.56 ± 0.65	85.65 ± 0.72	79.43 ± 0.58	74.16 ± 0.43	105.15
4j	93.56 ± 0.68	88.97 ± 0.73	83.56 ± 0.89	78.85 ± 0.96	75.36 ± 0.99	116.22
4k	79.18 ± 0.42	76.84 ± 0.58	74.34 ± 0.55	67.73 ± 0.63	63.12 ± 0.39	85.02
4l	93.89 ± 0.52	87.75 ± 0.56	81.43 ± 0.65	78.36 ± 0.43	72.55 ± 0.29	102.29

interactions are hydrophobic in major and the protein−ligand interactions at the binding domain cavity were studied from ligand interaction studies on molecular operating environment (MOE) software. The study revealed that all compounds are well interacted with the specified proteins of the target cells in the binding domains of the human ribonucleotide reductase, and this study has helped to identify the human ribonucleotide reductase inhibitors; the data is presented in Tables 5 and 6.

The *in silico* study performed has helped to screen a large number of newly proposed compounds to assess the potential inhibitory activity theoretically by docking onto the selected targets. The resulted docking scores and modules infer us to proceed for *in vitro* assays for a validated cell inhibitory activity. Ultimately, the more stabilized conformations have been further considered for studying QSAR (quantitative structure−activity relationship) descriptors followed by Lipinski filtration to identify drug likeliness and interactions of **4a−l** with novel inhibitors with the ABAD active site.

The molecular docking of **4a−l** against the human ribonucleotide reductase active site (PDB ID: 3HNC) revealed the arene−arene interactions of **4a**, **4c**, and **4h** with Tyr625, P═O interactions of **4b** with Asn144, P−OH interactions of **4b** with Gln609, **4e** and **4f** with Glu615, thiadiazolic sulfur interactions of **4c** with Thr626, **4j** with Phe146 and **4g** with

Table 4. Percentage of PANC-1Cell Survival Studies with SAHA Derivatives

entry	concentrations					IC$_{50}$ (μg/mL)
	3.125 μM	6.25 μM	12.5 μM	25.0 μM	50.0 μM	
4a	90.76 ± 0.95	83.52 ± 0.54	75.77 ± 1.06	63.93 ± 0.87	58.42 ± 0.72	57.08
4b	92.61 ± 0.46	84.88 ± 0.59	76.86 ± 0.73	64.87 ± 0.63	57.67 ± 0.78	55.66
4c	93.78 ± 1.27	85.69 ± 0.19	74.36 ± 0.49	67.58 ± 0.23	63.92 ± 0.57	67.21
4d	94.42 ± 0.78	88.69 ± 0.65	81.93 ± 0.52	76.58 ± 0.37	72.66 ± 0.48	218.16
4e	99.91 ± 0.85	96.33 ± 0.56	94.25 ± 0.79	92.18 ± 0.83	89.71 ± 0.65	258.74
4f	99.41 ± 0.38	97.75 ± 0.54	96.13 ± 0.42	94.76 ± 0.37	91.85 ± 0.59	332.59
4g	98.02 ± 0.55	91.15 ± 0.73	89.60 ± 0.41	88.04 ± 0.39	85.50 ± 0.65	221.08
4h	95.71 ± 0.48	91.58 ± 0.43	89.13 ± 0.37	88.01 ± 0.62	86.05 ± 0.53	262.37
4i	99.54 ± 0.75	95.69 ± 0.66	90.47 ± 0.62	88.89 ± 0.59	85.97 ± 0.79	188.16
4j	97.33 ± 0.98	93.67 ± 0.87	89.43 ± 0.76	84.69 ± 0.65	79.54 ± 0.93	129.54
4k	88.15 ± 0.65	82.26 ± 0.48	74.86 ± 0.35	66.52 ± 0.39	54.92 ± 0.52	54.31
4l	99.87 ± 0.63	93.14 ± 0.87	87.28 ± 0.74	82.27 ± 0.35	77.54 ± 0.72	110.24
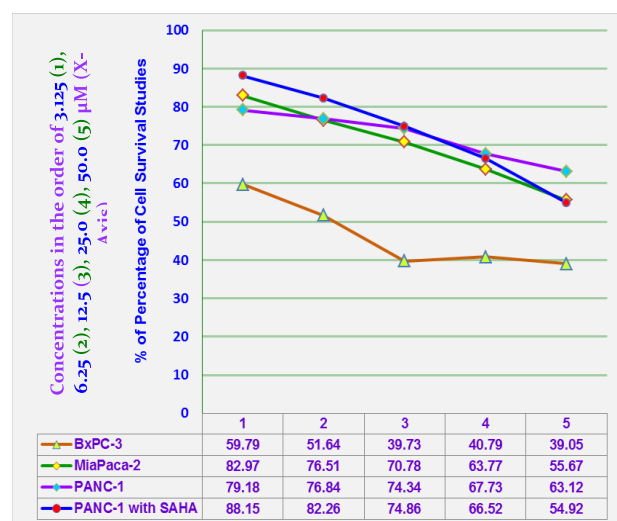
Figure 4. Effect of **4k** and **4k**+SAHA against BxPC-3, Panc-1 and Miapaca-2, and Panc-1 cells.

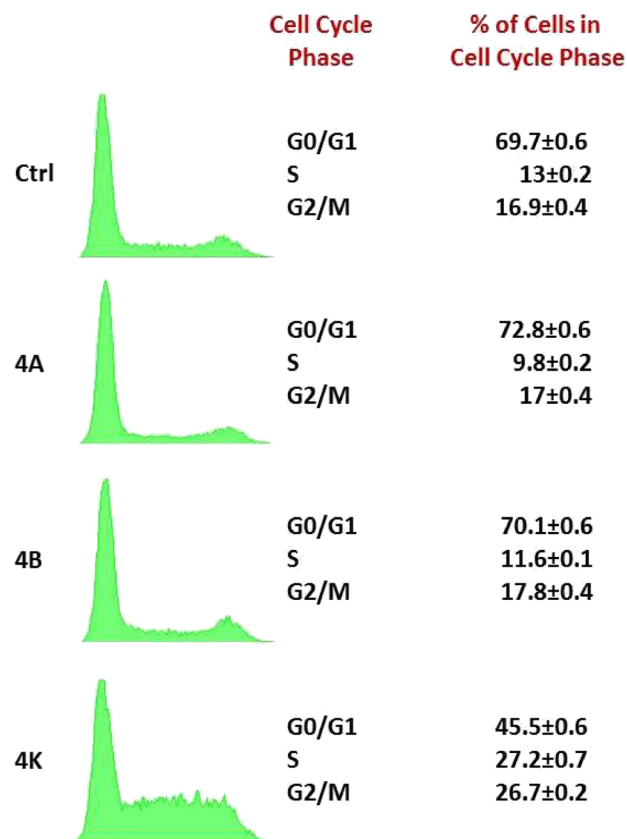**Figure 5.** Effects of title compounds on the cell cycle of BxPC-3.

Figure 6. Two-dimensional ligand−receptor interaction representation maps.

Gln609 and Thr150, arene−H interactions of **4f** and **4j** with Gln609, thiadiazole ring−arene interactions of **4f** with Tyr625, thiadiazolic−SH interactions of **4g** with Arg628 and Thr150, thiazole ring−H interactions of **4h** with Asn614, triazolic−NH interactions of **4h** with Thr621, triazole ring mediated −P−CH−NH interactions of **4h** with Glu615, and −NO$_2$ interactions of **4h** and **4f** with Tyr625, which confirms their docking modes with target receptor proteins. Similarly, the molecular docking of **4a**−**l** against histone deacetylase (HDAC, PDB ID: 4LXZ) revealed the P═O interactions of **4a**, **4d**, and **4l** with His142, **4e** with His180, **4g** and **4k** with Tyr100, **4h** with His142, **4i** with Lys33, **4j** with Tyr306, and **4k** with Tyr100, −P(O)OH interactions of **4b** and **4h** with Asp178, **4g**, **4i**, and **4l** with Tyr100, **4h** with Asp267, **4k** with Lys33, thiadiazolic−N$_3$ interactions of **4a** with arene-mediated Phe208 and His180, **4e** with Phe152, **4e**, **4f**, and **4j** with Asp101 and Phe208, thiadiazole−arene interactions of **4j** with Phe208 and Asp101, triazole ring−arene interactions of **4d**, **4h**, and **4l** with Phe152, **4h** and **4l** with His180, P(O)−O−C$_{Ar}$ interactions of **4f** with His180, thiadiazolic−2-SH-mediated arene interactions of **4g** with Phe152 and Asp101, triazolic−5-NH interactions of **4h** with Tyr306, diethylamino methylic−arene interactions of **4i** with Phe208, P(O)−O−C$_{Ar}$ ring interactions of **4j** with His180, and 2-mercapto thiadiazole−

arene interactions of **4k** with Phe152 and Asp101, which confirms their docking with target receptors.

In continuation, the molecular docking analysis of SAHA derivatives of **4a**−**l** against histone deacetylase (HDAC, PDB ID: 4LXZ) revealed the main interactions *viz.*, C(O)−NH− interactions (**4a** and **4b**: Tyr306, **4d**: Phe208, **4e**: Asp101, **4g**: His143, **4i**: Tyr100, and **4l**: Tyr306), −O−NH− interactions

Table 5. Molecular Docking Interaction of 4a−l against Human Ribonucleotide Reductase Active Site

[a]entry	[b]docking score	[c]no. H bonds	[d]interacting residues of ABAD
4a	−4.936	arene interaction	Tyr 625
4b	−4.543	1	Gln 609
4c	−5.075	2	Try 625, Thr 626
4d	−4.187	1	Asn 144
4e	−5.212	1 and 3	Gln 615 and Gln 615, Try 625, Gln 609
4f	−5.589	arene interaction	Try 625
4g	−5.303	4	Arg 628, 2 (Thr 150), Gln 609
4h	−5.361	3 and arene interaction	Glu 615, Thr 621, Tyr 625 and Asn 614, Tyr 625
4i	−5.212		
4j	−5.873	2	Phe 146, Gln 609
4k	−5.352		
4l	−5.271		

[a]The novel 3HNC inhibitors. [b]Docking scores predicted from MOE docking in binding domain of docked novel leads and ribonucleotide reductase proteins. [c]Number of hydrogen bonds formed in binding domain among ribonucleotide reductase and the novel leads. [d]The active site residues interacting among ribonucleotide reductase protein and the novel inhibitors in the ligand−receptor complex of the study.

(4a, 4b, and 4h: Asp101, 4d: His180, 4f: Phe208, and 4f and 4 h: Phe152), arene interactions (4c: His180, 4g: Lys33), 2-mercapto thiadiazolic interactions (4c: Asp101), 2-mercapto thiadiazolic−arene interactions (4c: Phe152), P−O−C$_{Ar}$ interactions (4c: Tyr306), P=O interactions (4d: Tyr306, 4h: Lys33, and 4k: Tyr100), triazole−arene interactions (4d: Phe152), triazolic−NH interactions (4d: Gly151, 4l: Asp101), thiadiazole interactions (4e: Asp101), thiadiazolic S-arene interactions (4e: Phe152), thiadiazole arene interactions (4f: Phe208), thiazolic N interactions (4i: Asp101), thiazolic N-arene interactions (4i: Phe208), thiazolic NH interactions (4i: Gly151), thiazolic NH-arene interactions (4i: Phe152), diethylamino methyl interactions (4i and 4j: Asp267 and Asp178), diethylamino methyl−arene interactions (4i and 4j: His142), and thiadiazolic S interactions (4j: Asp101) with target receptors (Table 7).

ADMET Properties. ADMET (absorption, distribution,-metabolism, and excretion) properties of 4a−l revealed 4a, 4b, and 4i−l as potent and 4c−h are moderate with intestinal absorption, and all have medium permeability for *in vitro* Caco-2 cells, low permeability for *in vitro* MDCK cells, low absorption with *in vivo* blood−brain barrier (BBB) penetration capacity, and supported them as CNS-active compounds as they are penetrable to BBB. The extent of plasma protein binding (PPB) of a compound stimulates the drug action as well as the compound's disposition and efficacy. Based on the ADMET properties, the percentage of drug compound bound with plasma proteins was envisioned and here compounds 4c, 4g, and 4i−l were strongly bound, whereas compounds 4a, 4b, 4d, 4e, and 4f are identified as weakly bound to plasma proteins (Table 8).

QSAR Studies. The understanding of chemical interactions of compounds with the anticipated pharmacological target helps in ascertaining their use as potential drugs.[50,51] Hence, the prediction of molecular descriptors for 4a−l from the QSAR study proved them as safer drugs in acceptable range of values. The molecular weights of 4a−l are less than 500
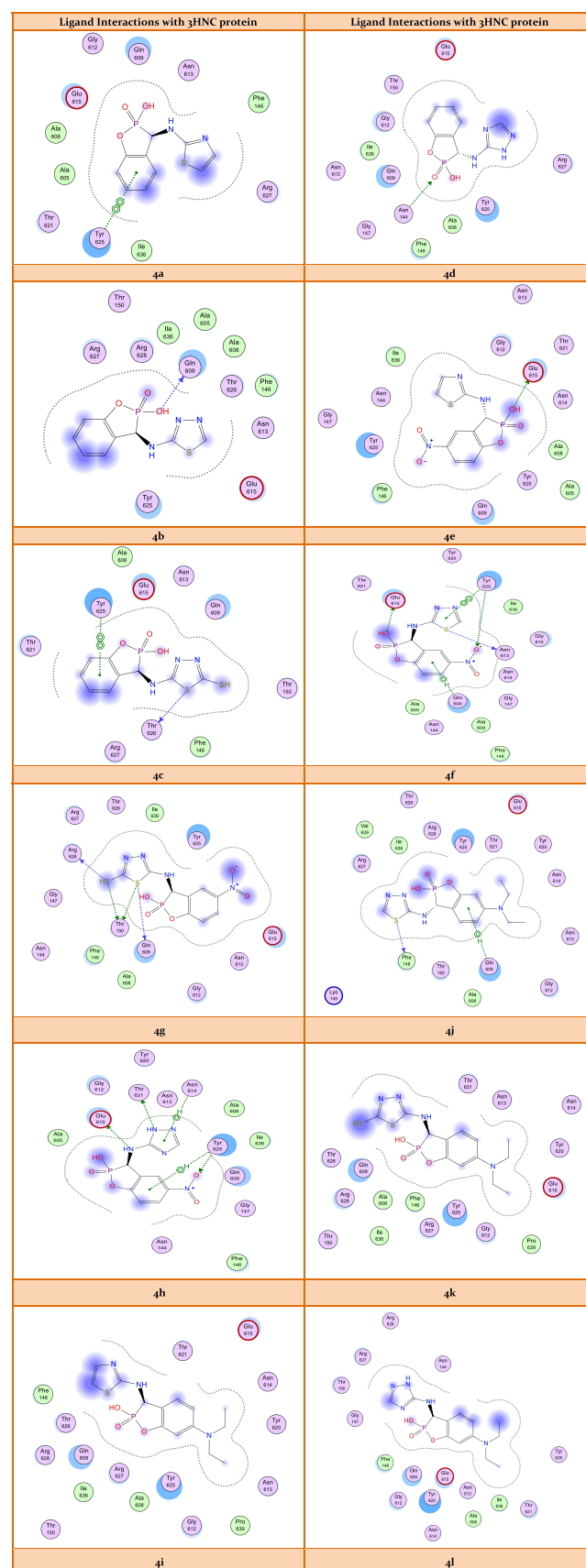
Table 6. Molecular Docking Interactions 4a−l with 3HNC Protein at the Human Ribonucleotide Reductase Active Site

Table 7. Comparative Protein−Ligand Binding Properties of 4a−l and Their SAHA Derivatives

	docking score		binding energy		binding affinity Pki		efficiency	
entry	pure compound	SAHA derivative	pure compound	SAHA derivative	pure compound	SAHA derivative	pure compound	SAHA derivative
4a	−12.5	−11.9	−18.7	−28.9	10.2	11.70	0.605	0.335
4b	−13.8	−11.7	−19.0	−7.70	10.4	10.70	0.612	0.306
4c	−12.0	−12.0	−9.40	10.20	8.20	11.20	0.459	0.314
4d	−14.6	−13.0	−23.0	−19.80	8.70	11.17	0.517	0.319
4e	−10.0	−10.7	−9.22	495.0	6.05	2.700	0.303	0.070
4f	−13.2	−12.3	−7.30	−28.04	8.46	10.90	0.420	0.289
4g	−12.1	−13.0	−0.949	−30.2	8.10	11.02	0.390	0.290
4h	−13.5	−13.8	−19.80	−24.7	9.40	11.42	0.474	0.300
4i	−11.0	−12.5	−14.20	−29.4	6.60	12.20	0.302	0.305
4j	−13.3	−13.4	−5.90	−22.46	9.90	14.30	0.434	0.359
4k	−11.6	−12.4	−5.80	12.50	7.60	9.600	0.334	0.230
4l	−14.0	−15.25	−12.1	−37.044	9.80	12..88	0.448	0.322

Table 8. ADMET Properties Predicted for Compounds 4a−l

entry	human intestinal absorption (HIA, %)[a]	in vitro Caco-2 cell permeability (nm/sec)[b]	in vitro MDCK cell permeability (nm/sec)[c]	in vitro skin permeability (logKp, cm/hour)[d]	in vitro plasma protein binding (%)[e]	in vivo blood−brain barrier penetration (C.brain /C.blood)[f]	toxicity[g]
4a	86.3824	1.3408	26.8358	−3.7287	82.6676	0.2629	negative
4b	75.6539	0.4007	21.2933	−4.1593	83.0199	0.1383	negative
4c	64.2959	0.3780	32.3669	−3.6705	99.0693	0.1129	negative
4d	65.52749	0.3749	10.6479	−4.4693	73.3206	0.3142	negative
4e	44.9103	0.3733	1.5565	−3.5385	84.2593	0.0980	negative
4f	28.6676	0.3736	0.8129	−3.8568	81.0702	0.0685	negative
4g	20.0169	0.3695	0.7395	−3.5409	99.7054	0.0593	negative
4h	20.8803	0.3673	1.2663	−4.1431	67.6284	0.3162	negative
4i	92.1140	18.2471	69.1110	−2.9966	100.0000	0.4244	negative
4j	85.3032	5.3632	52.2455	−3.3667	100.0000	0.2141	negative
4k	76.8665	1.4893	10.7085	−3.1303	100.0000	0.1683	negative
4l	76.0095	1.1041	82.9175	−3.8803	97.1879	0.1495	negative

[a]HIA is the sum of bioavailability and absorption evaluated from the ratio of excretion or cumulative excretion in urine, bile, and feces. [b]Caco-2 cells are derived from human colon adenocarcinoma and possess multiple drug transport pathways through the intestinal epithelium. [c]MDCK cell system is used as a tool for rapid permeability screening. [d]The in vitro skin permeability infers the transdermal drug delivery property. [e]The percent of drug binds to plasma protein. [f]Blood−brain barrier (BBB) = [brain]/[blood]. [g]In vitro Ames test by metabolic and non-metabolic activated TA100 and TA1535 strains collected from rat liver homogenate.

Daltons and logP values below 5 units govern themselves in a safe manner with an *in vivo* host. The number of hydrogen bond acceptors and donors present in them strengthens the formation of the best ligand−receptor complex pair. The congruent sum-up of these parameters persuades Lipinski's rule of five and ascertains their inherent pharmacological potentiality. Their surface area and volume values ensure their absorption and distribution in the best interaction with the host system.

Other parameters like gradient energy and total energy have confirmed the establishment of their interactions with receptor proteins and their capability to fit into the target's binding cavity. Ultimately, the binding region of the receptor protein, volume, molar refractivity, hydration energy, polarizability, and conformation has empowered the interaction of **4a−l** with the receptor. In support of *in vitro* studies, the 2D-QSAR studies were accomplished by using the three eigenvectors (PCA1, PCA2, and PCA3) and their linear regression studies are plotted in Figure 7 and noticed that the most potent curves are identified nearer the correlation curve; the molecular descriptors are shown in Table 9. The 2D-QSAR analysis revealed that all the values are laid in the +3 to −3 range, and the study supported the effective drug properties of **4a, 4b,** and **4k** (Figure 8).
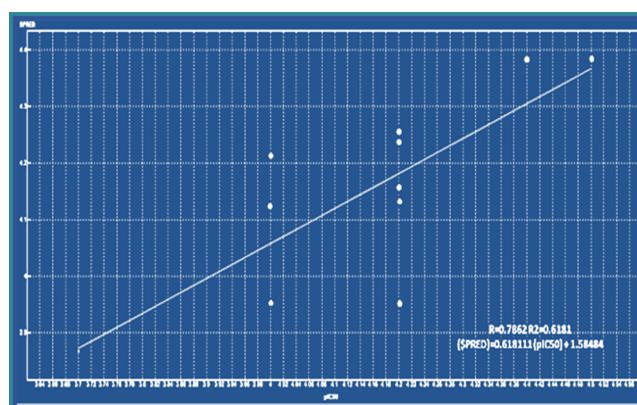

Figure 7. Linear correlation curves of the synthesized compounds.

Bioactivity and Toxicity Risk Studies. The bioactivity study results revealed them as potential inhibitors toward ion channel modulator and G protein-coupled receptor ligand and also proved them as good inhibitors of protease, kinase, enzyme, and nuclear receptor ligand. Similarly, they are good with drug score and drug-likeness values along with the hydration energy gradient energy and total energy values. The

Table 9. Molecular Descriptors of Compounds 4a−l from the QSAR Study[a]

entry	Lipinski parameters						Veber parameters			other molecular parameters						
	M_W	HB Don	HBAcc	logP (o/w)	MR	Lip. Vio.	TPSA	no. of RB	Veb. Vio.	no. of H	V.Vol.	ρ	S	CLP	% ABS	P
4a	268.23	5	2	1.32	63.62	0	71.45	2	0	19	168.53	1.59	−2.69	0.17	84.35	22.84
4b	269.22	6	2	0.98	61.42	0	84.34	2	0	17	201.59	1.66	−2.13	−0.5	79.90	22.87
4c	301.29	6	2	1.50	69.27	0	84.35	2	0	18	219.25	1.71	−3.85	−0.01	79.89	25.73
4d	252.17	7	3	0.04	57.21	0	100.14	2	0	16	195.86	1.66	−2.18	−1.32	74.45	36.90
4e	313.23	8	2	1.26	69.66	0	117.28	3	0	18	229.08	1.73	−3.15	−0.76	68.53	25.26
4f	314.22	9	2	0.92	67.46	0	130.17	3	0	16	224.92	1.81	−2.59	−1.42	64.10	24.25
4g	346.29	9	2	1.44	75.30	0	130.16	3	0	17	242.58	1.85	−4.31	−0.93	64.09	27.55
4h	297.17	10	3	−0.02	63.24	0	145.96	3	0	15	219.20	1.82	−2.64	−2.24	58.64	22.91
4i	339.36	6	2	2.15	86.02	0	74.69	5	0	32	285.25	1.41	−3.33	0.88	83.23	32.24
4j	340.35	7	2	1.81	83.82	0	87.58	5	0	30	281.10	1.46	−2.77	0.21	78.78	34.53
4k	372.41	7	2	2.33	91.67	0	87.59	5	0	31	298.76	1.51	−4.48	0.74	78.77	34.56
4l	323.29	8	3	0.87	79.60	0	103.87	5	0	29	275.37	1.45	−2.82	−0.61	73.16	29.88

[a]M_W: molecular weight; HB Don: hydrogen bond donors (n ON); HB Acc: hydrogen bond acceptors (n OH NH); logP: log of octanol to water partition coefficient; MR: molecular refractivity (cm^3/mol); Lip. Vio.: Lipinski violations; TPSA: total polar surface area (A°)^2; no. of RB: number of rotatable bonds; Veb. Vio.: Veber violations; no. of "H": number of hydrophobic atoms; V.vol.: van der Waals volume; ρ: density (g/cc); S: solubility; CLP: ClogP; % ABS: % of absorption; P: polarizability (A^{o3}).
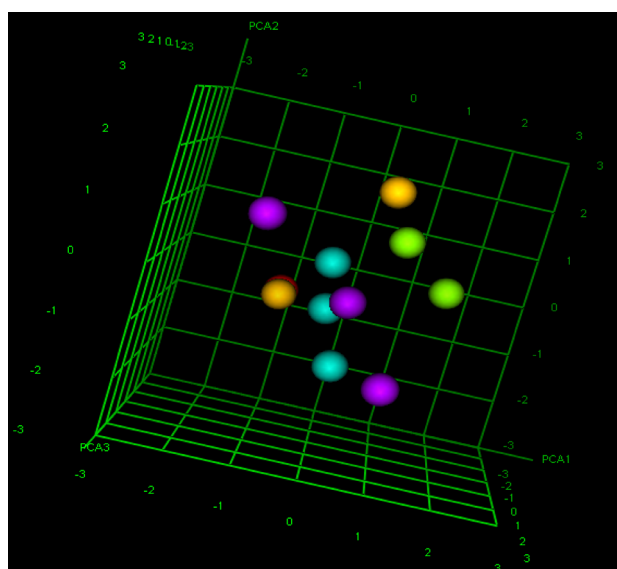

Figure 8. 2D-QSAR principal component analysis (PCA) plots of compounds **4a−l** against the BxPC-3 cell.

toxicity risk analysis reveals them as negative toward mutagenic, tumorigenic, irritant (Table 10), and reproductive effects and supports them as drug proficient compounds.

CONCLUSIONS

Synthesis of a class of 3-amino-2-hydroxybenzofused 2-phospha-γ-lactones (**4a−l**) has been accomplished and reported them as potential Panc-1, Miapaca-2, and BxPC-3 pancreatic cell growth inhibitors from the *in vitro* anti-pancreatic cell proliferation assay and from the predicted molecular docking and 3D-QSAR properties. In addition, the MTT assay performed for the prepared SAHA derivatives of **4a-l** has also supported them as potential anti-pancreatic cancer active compounds and also identified them as potential histone deacetylase (HDAC) inhibitors. The potential anti-pancreatic cancer cell proliferative activity identified from the cell cycle analysis of **4k** by flow cytometry at low micromolar concentrations prompted the authors to report the title

compounds as potential inhibitors as ascertained by the *S* phase cell cycle arrest. This significant rationale has enriched our study to develop some more new 3-amino-2-hydroxybenzofused 2-phospha-γ-lactones and to report them as potential HDAC inhibitors. Ultimately, this study will definitely enhance the research thrust in the development of new and innovative medicinal applications of organophosphorus heterocycles as anticancer agents. Explicitly, these detailed biological studies surely help in developing new organophosphorus heterocycles and establishing their structure−reactivity relationship and will pave the way for the discovery of newer drugs.

EXPERIMENTAL SECTION

General. Chemicals, reagents, and solvents were procured from Merck, where the solvents used for spectroscopy and other characterization of studies were reagent grade. NMR spectra were recorded on a Bruker instrument at 400 MHz for ^{1}H NMR and 100 MHz for ^{13}C NMR in CDCl$_3$ solution using TMS as an internal standard. Chemical shifts were given in ppm, and coupling constants (*J*) were given in Hz. LCMS mass spectral characterization was performed by using a Jeol SX 102 DA/600 mass spectrometer; FTIR spectral analysis was performed on Bruker Alpha featured with an EcoATR interferometer equipped with a single reflection sampling module and ZnSe crystal, and absorption maxima readings were given in wavenumbers (cm$^{−1}$). Melting points were recorded on EZ-Melt automated equipment.

Chemistry. Title compounds (**4a−l**) were synthesized by reacting 0.10 mL of 2-hydroxybenzaldehye (1.0 mmol), 0.10 g of 2-aminothiazole (1.0 mmol), and 0.23 mL of diphenylphosphite (1.2 mmol) in 6 mL of toluene in a 50 mL flask fitted with a reflux condenser, the contents were refluxed to completion of the reaction by TLC monitoring (3:7 ratio of ethyl acetate and hexane), and the reaction was completed by the product formation after 3 h of refluxing. After completion of the reaction, contents of the flask were cooled to room temperature, then added 5 mL of methanol, and then filtered. The filtered residue was washed with 5 mL of methanol four times and then purified on a chromatographic column and collected the solid in pure form and then dried in a vacuum

Table 10. Bioactivity Scores, Drug Properties, and Toxicity Risks of 7a−s[a]

entry	bioactivity						drug properties		energy parameters			toxicity risks			
	GPCRL	ICM	KI	NRL	PI	EI	drug-likeness	drug score	H.E.	G.E.	T.E.	Mut	Tum	Irrit	R.E.
7a	−0.27	0.19	0.09	−0.40	0.25	0.45	−23.67	0.46	−19.14	0.091	73.50	Nil	Nil	Nil	Nil
7b	−0.51	−0.02	−0.11	−0.27	0.05	0.31	−23.16	0.28	−19.15	0.093	73.51	Nil	Nil	Nil	Nil
7c	−0.74	−0.28	−0.15	−0.58	0.23	0.43	−24.68	0.42	−20.28	0.097	82.70	Nil	Nil	Nil	Nil
7d	−0.31	0.04	−0.03	−0.90	0.07	0.31	−21.99	0.47	−14.98	0.097	78.22	Nil	Nil	Nil	Nil
7e	−0.32	0.09	0.05	−0.32	0.16	0.28	−30.14	0.44	−22.08	0.098	98.84	Nil	Nil	Nil	Nil
7f	−0.51	−0.09	−0.12	−0.20	−0.01	0.16	29.73	0.27	−25.02	0.099	97.07	Nil	Nil	Nil	Nil
7g	−0.72	−0.33	−0.17	−0.50	0.14	0.25	−31.23	0.39	−24.93	0.099	100.91	Nil	Nil	Nil	Nil
7h	−0.34	−0.04	−0.05	−0.75	0.01	0.16	−28.52	0.46	−26.53	0.098	95.14	Nil	Nil	Nil	Nil
7i	−0.02	0.11	0.27	−0.15	0.32	0.32	−24.92	0.43	−13.78	0.094	123.59	Nil	Nil	Nil	Nil
7j	−0.20	−0.06	0.12	−0.05	0.17	0.21	−24.56	0.27	−18.60	0.096	121.20	Nil	Nil	Nil	Nil
7k	−0.42	−0.27	0.04	−0.34	0.29	0.28	−26.17	0.37	−18.06	0.096	121.22	Nil	Nil	Nil	Nil
7l	−0.04	−0.01	0.18	−0.54	0.19	0.21	−23.42	0.45	−19.49	0.094	122.26	Nil	Nil	Nil	Nil

[a]GPCRL: G protein-coupled receptor ligand; ICM: ion channel modulator; KI: kinase inhibitor; NRL: nuclear receptor ligand; PI: protease inhibitor; EI: enzyme inhibitor; H.E.: hydration energy (kcal/mol); G.E.: gradient energy (kcal/molA°); T.E.: total energy (kcal/mol); Mut: mutagenic; Tum: tumorigenic; Irrit: irritant; and R.E.: reproductive effect.

oven to get **4a** in pure form. Similarly, the remaining compounds **4b−l** were synthesized by varying the substrate and they were structurally ascertained by the spectral and elemental characterization studies.

2-Hydroxy-3-(1,3-thiazol-2-ylamino)-2,3-dihydro-1,2λ⁵-benzoxaphosphol-2-one (4a). Brownish pink solid, yield: 79.2%, mp: 285−287 °C; IR (ZnSe) ν (cm^{-1}): 1076 (P−O), 1225 (P=O), 3427 (N−H); ^{1}H NMR (400 MHz, DMSO-d_6) δ: 3.98 (*s*, 1H, H-3), 4.25 (*s*, 1H, H-10), 6.77 (*d*, 1H, H-12), 6.90−6.84 (*m*, 2H, H-5, and H-7), 7.09−7.03 (*m*, 2H, H-4, and H-6), 7.24 (*d*, 1H, H-13) ppm; ^{13}C NMR (100 MHz, DMSO-d_6) δ: 64.3 (C-3), 112.5 (C-13), 119.4 (C-7), 121.2 (C-5), 128.2 (C-6), 128.4 (C-4), 129.8 (C-8), 137.2 (C-14), 155.6 (C-9), 163.4 (C-11) ppm; ^{31}P NMR (160 MHz, DMSO-d_6) δ: 17.69 ppm; ESI MS *m/z*: 537.1 [2 M + H]$^+$, 269.2 [M + H]$^+$; anal. calcd for C$_{10}$H$_9$N$_2$O$_3$PS: C, 44.78; H, 3.38; N, 10.44. Found: C, 44.60; H, 3.33; N, 10.38.

2-Hydroxy-3-(1,3,4-thiadiazol-2-ylamino)-2,3-dihydro-1,2λ⁵-benzoxaphosphol-2-one (4b). Pale pink solid, yield: 75.7%, mp: 269−271 °C; IR (ZnSe) ν (cm^{-1}): 1085 (P−O), 1239 (P=O), 3417 (N−H); ^{1}H NMR (400 MHz, DMSO-d_6) δ: 3.97 (s, 1H, H-3), 4.24 (s, 1H, H-10), 6.92−6.86 (m, 2H, H-5, and H-7), 7.08−7.02 (m, 2H, H-4, and H-6), 8.75 (s, 1H, H-13) ppm; ^{13}C NMR (100 MHz, DMSO-d_6) δ: 64.1 (C-3), 119.5 (C-7), 121.3 (C-5), 128.4 (C-6), 128.2 (C-4), 129.9 (C-8), 152.3 (C-13), 156.7 (C-9), 164.3 (C-11) ppm; ^{31}P NMR (160 MHz, DMSO-d_6) δ: 16.56 ppm; ESI MS *m/z*: 539.5 [2 M + H]$^+$, 270.2 [M + H]$^+$; anal. calcd for C$_9$H$_8$N$_3$O$_3$PS: C, 40.15; H, 3.00; N, 15.61. Found: C, 39.97; H, 2.95; N, 15.48.

2-Hydroxy-3-[(5-sulfanyl-1,3,4-thiadiazol-2-yl)amino]-2,3-dihydro-1,2λ⁵-benzoxaphosphol-2-one (4c). Reddish pink solid, yield: 69.2%, mp: 257−259 °C; IR (ZnSe) ν (cm^{-1}): 1089 (P−O), 1229 (P=O), 3420 (N−H); ^{1}H NMR (400 MHz, DMSO-d_6) δ: 3.25 (s, 1H, C$_{13}$-SH), 3.94 (s, 1H, H-3), 4.25 (s, 1H, H-10), 6.93−6.87 (m, 2H, H-5, and H-7), 7.07−7.03 (m, 2H, H-4, and H-6) ppm; ^{13}C NMR (100 MHz, DMSO-d_6) δ: 64.3 (C-3), 119.6 (C-7), 121.7 (C-5), 128.4 (C-6), 128.6 (C-4), 129.7 (C-8), 156.4 (C-9), 164.6 (C-11), 179.3 (C-13) ppm; ^{31}P NMR (160 MHz, DMSO-d_6) δ: 17.94 ppm; ESI MS *m/z*: 602.6 [2 M + H]$^+$; 301.8 [M + H]$^+$; anal. calcd for C$_9$H$_8$N$_3$O$_3$PS$_2$: C, 35.88; H, 2.68; N, 13.95. Found: C, 35.63; H, 2.62; N, 13.82.

2-Hydroxy-3-(1H-1,2,4-triazol-3-ylamino)-2,3-dihydro-1,2λ⁵-benzoxaphosphol-2-one (4d). White solid, yield: 73.6%, mp: 285−287 °C; IR (ZnSe) ν (cm^{-1}): 1089 (P−O), 1237 (P=O), 3429 (N−H); ^{1}H NMR (400 MHz, DMSO-d_6) δ: 3.96 (s, 1H, H-3), 4.25 (s, 1H, H-10), 6.93−6.87 (m, 2H, H-5, and H-7), 7.09−7.03 (m, 2H, H-4, and H-6), 7.63 (s, 1H, H-14), 12.85 (s, 1H, C$_{14}$-NH$_{Ar}$) ppm; ^{13}C NMR (100 MHz, DMSO-d_6) δ: 64.5 (C-3), 119.3 (C-7), 121.4 (C-5), 128.3 (C-6), 128.6 (C-4), 129.9 (C-8), 146.3 (C-14), 156.2 (C-9), 163.6 (C-11) ppm; ^{31}P NMR (160 MHz, DMSO-d_6) δ: 18.89 ppm; ESI MS *m/z*: 505.1432 [2 M + H]$^+$, 253.0715 [M + H]$^+$; anal. calcd for C$_9$H$_9$N$_4$O$_3$P: C, 42.87; H, 3.60; N, 22.22. Found: C, 42.58; H, 3.55; N, 22.10.

2-Hydroxy-5-nitro-3-(1,3-thiazol-2-ylamino)-2,3-dihydro-1,2λ⁵-benzoxaphosphol-2-one (4e). Brownish yellow solid, yield: 86.5%, mp: 237−239 °C; IR (ZnSe) ν (cm^{-1}): 1078 (P−O), 1218 (P=O), 3417 (N−H); ^{1}H NMR (400 MHz, DMSO-d_6) δ: 3.98 (s, 1H, H-3), 4.26 (s, 1H, H-10), 6.78 (d, 1H, H-13), 7.12 (d, 1H, H-7), 7.28 (d, 1H, H-14), 7.94 (d, 1H, H-6), 7.98 (s, 1H, H-4) ppm; ^{13}C NMR (100 MHz, DMSO-d_6) δ: 63.4 (C-3), 112.3 (C-13), 116.7 (C-7), 124.3 (C-6), 124.9 (C-4), 130.6 (C-8), 137.3 (C-14), 140.5 (C-5), 162.3 (C-9), 163.4 (C-11) ppm; ^{31}P NMR (160 MHz, DMSO-d_6) δ: 16.36 ppm; ESI MS *m/z*: 625.8 [2 M + H]$^+$; 313.9 [M + H]$^+$; anal. calcd for C$_{10}$H$_8$N$_3$O$_5$PS: C, 38.35; H, 2.57; N, 13.42. Found: C, 38.12; H, 2.53; N, 13.32.

2-Hydroxy-5-nitro-3-(1,3,4-thiadiazol-2-ylamino)-2,3-di-hydro-1,2λ⁵-benzoxaphosphol-2-one (4f). Pale brown solid, yield: 83.7%, mp: 249−251 °C; IR (ZnSe) ν (cm^{-1}): 1081 (P−O), 1226 (P=O), 3416 (N−H); ^{1}H NMR (400 MHz, DMSO-d_6) δ: 3.98 (s, 1H, H-3), 4.27 (s, 1H, H-10), 7.05 (d, 1H, H-7), 7.92 (d, 1H, H-6), 7.96 (s, 1H, H-4), 9.25 (s, 1H, H-13) ppm; ^{13}C NMR (100 MHz, DMSO-d_6) δ: 63.4 (C-3), 116.7 (C-7), 124.5 (C-6), 124.6 (C-4), 130.2 (C-8), 140.7 (C-5), 152.4 (C-13), 162.3 (C-9), 164.5 (C-11) ppm; ^{31}P NMR (160 MHz, DMSO-d_6) δ: 19.58 ppm. ESI MS *m/z*: 628.4 [2 M + H]$^+$; 314.7 [M + H]$^+$; anal. calcd for C$_9$H$_7$N$_4$O$_5$PS: C, 34.40; H, 2.25; N, 17.83. Found: C, 34.13; H, 2.19; N, 17.70.

2-Hydroxy-5-nitro-3-[(5-sulfanyl-1,3,4-thiadiazol-2-yl)-amino]-2,3-dihydro-1,2λ⁵-benzoxaphosphol-2-one (4g). Yellow solid, yield: 79.1%, mp: 224−226 °C; IR (ZnSe) ν (cm^{-1}): 1084 (P−O), 1226 (P=O), 3422 (N−H); ^{1}H NMR (400 MHz, DMSO-d_6) δ: 3.32 (s, 1H, C$_{13}$-SH), 3.98 (s, 1H, H-3),

4.28 (s, 1H, H-10), 7.14 (d, 1H, H-7), 7.93 (d, 1H, H-6), 7.98 (s, 1H, H-4) ppm; ^{13}C NMR (100 MHz, DMSO-d_6) δ: 63.2 (C-3), 116.9 (C-7), 123.8 (C-6), 124.4 (C-4), 130.7 (C-8), 140.5 (C-5), 162.4 (C-9), 164.6 (C-11), 184.5 (C-13) ppm; ^{31}P NMR (160 MHz, DMSO-d_6) δ: 17.36 ppm. ESI MS m/z: 692.8 [2 M + H]$^+$, 346.9 [M + H]$^+$; anal. calcd for C$_9$H$_7$N$_4$O$_5$PS$_2$: C, 31.22; H, 2.04; N, 16.18. Found: C, 31.01; H, 1.99; N, 16.13.

2-Hydroxy-5-nitro-3-(1H-1,2,4-triazol-3-ylamino)-2,3-dihydro-1,2λ⁵-benzoxaphosphol-2-one (4h). Yellow solid, yield: 82.4%, mp: 227−229 °C; IR (ZnSe) ν (cm^{-1}): 1094 (P−O), 1233 (P=O), 3431 (N−H); ^{1}H NMR (400 MHz, DMSO-d_6) δ: 7.64 (s, 1H, H-14), 3.98 (s, 1H, H-3), 4.25 (s, 1H, H-10), 7.14 (d, 1H, H-7), 7.92 (d, 1H, H-6), 7.98 (s, 1H, H-4), 12.95 (s, 1H, C$_{14}$-NH) ppm; ^{13}C NMR (100 MHz, DMSO-d_6) δ: 63.6 (C-3), 116.5 (C-7), 124.3 (C-6), 124.7 (C-4), 130.4 (C-8), 140.3 (C-5), 146.5 (C-14), 162.3 (C-9), 163.4 (C-11) ppm; ^{31}P NMR (160 MHz, DMSO-d_6) δ: 17.45 ppm; ESI MS m/z: 298.3 [M + H]$^+$, 598.6 [2 M + H]$^+$; anal. calcd for C$_9$H$_8$N$_5$O$_5$P: C, 36.38; H, 2.71; N, 23.57, Found: C, 36.14; H, 2.67; N, 23.42.

6-(Diethylamino)-2-hydroxy-3-(1,3-thiazol-2-ylamino)-2,3-dihydro-1,2λ⁵-benzoxaphosphol-2-one (4i). Lavender solid, yield: 75.3%, mp: 307−309 °C; IR (ZnSe) ν (cm^{-1}): 1095 (P−O), 1231 (P=O), 3423 (N−H); ^{1}H NMR (400 MHz, DMSO-d_6) δ: 1.24 (t, 6H, 2 × N-CH$_2$CH$_3$), 3.60 (q, 4H, 2 × N-CH$_2$CH$_3$), 3.98 (s, 1H, H-3), 4.24 (s, 1H, H-10), 6.18 (s, 1H, H-7), 6.24 (d, 1H, H-13), 6.78 (d, 1H, H-13), 6.89 (d, 1H, H-4), 7.24 (d, 1H, H-14) ppm; ^{13}C NMR (100 MHz, DMSO-d_6) δ: 12.7 (2 × N-CH$_2$-CH$_3$), 44.2 (2 × N-CH$_2$-CH$_3$), 64.5 (C-3), 98.6 (C-7), 105.8 (C-5), 112.4 (C-13), 119.3 (C-8), 129.5 (C-4), 137.5 (C-14), 149.4 (C-6), 156.7 (C-9), 163.8 (C-11) ppm; ^{31}P NMR (160 MHz, DMSO-d_6) δ: 18.25 ppm; ESI MS m/z: 679.4 [2 M + H]$^+$, 340.2 [M + H]$^+$; anal. calcd for C$_{14}$H$_{18}$N$_3$O$_3$PS: C, 49.55; H, 5.35; N, 12.38. Found: C, 49.30; H, 5.29; N, 12.27.

6-(Diethylamino)-2-hydroxy-3-(1,3,4-thiadiazol-2-ylamino)-2,3-dihydro-1,2λ⁵-benzoxaphosphol-2-one (4j). Pale pink solid, yield: 72.1%, mp: 256−258 °C; IR (ZnSe) ν (cm^{-1}): 1082 (P−O), 1238 (P=O), 3423 (N−H); ^{1}H NMR (400 MHz, DMSO-d_6) δ: 1.23 (t, 6H, 2 × N-CH$_2$CH$_3$), 3.55 (q, 4H, 2 × N-CH$_2$CH$_3$), 3.93 (s, 1H, H-3), 4.25 (s, 1H, H-10), 6.16 (s, 1H, H-7), 6.24 (d, 1H, H-13), 6.92 (d, 1H, H-4), 9.18 (s, 1H, H-13) ppm; ^{13}C NMR (100 MHz, DMSO-d_6) δ: 12.7 (2 × N-CH$_2$-CH$_3$), 47.2 (2 × N-CH$_2$-CH$_3$), 74.4 (C-3), 98.8 (C-7), 105.2 (C-5), 119.3 (C-8), 129.4 (C-4), 149.5 (C-6), 152.3 (C-13), 156.6 (C-9), 164.5 (C-11) ppm; ^{31}P NMR (160 MHz, DMSO-d_6) δ: 18.32 ppm; ESI MS m/z: 683.8 [2 M + H]$^+$, 341.4 [M + H]$^+$; anal. calcd for C$_{13}$H$_{17}$N$_4$O$_3$PS: C, 45.88; H, 5.03; N, 16.46. Found: C, 45.31; H, 4.99; N, 16.31.

6-(Diethylamino)-2-hydroxy-3-[(5-sulfanyl-1,3,4-thiadiazol-2-yl)amino]-2,3-dihydro-1,2λ⁵-benzoxaphosphol-2-one (4k). Yellow solid, yield: 67.8%, mp: 172−174 °C; IR (ZnSe) ν (cm^{-1}): 1096 (P−O), 1235 (P=O), 3428 (N−H); ^{1}H NMR (400 MHz, DMSO-d_6) δ: 1.28 (t, 6H, 2 × N-CH$_2$CH$_3$), 3.62 (q, 4H, 2 × N-CH$_2$CH$_3$), 3.98 (s, 1H, H-3), 4.25 (s, 1H, H-10), 6.18 (s, 1H, H-7), 6.24 (d, 1H, H-13), 6.92 (d, 1H, H-4), 13.16 (s, 1H, C$_{13}$-SH) ppm; ^{13}C NMR (100 MHz, DMSO-d_6) δ: 12.9 (2 × N-CH$_2$-CH$_3$), 47.4 (2 × N-CH$_2$-CH$_3$), 74.3 (C-3), 98.7 (C-7), 105.6 (C-5), 119.4 (C-8), 129.5 (C-4), 149.2 (C-6), 156.6 (C-9), 164.5 (C-11), 184.4 (C-13) ppm; ^{31}P NMR (160 MHz, DMSO-d_6) δ: 18.67 ppm; ESI MS m/z: 746.1 [2 M + H]$^+$, 373.5 [M + H]$^+$; anal. calcd for

C$_{13}$H$_{17}$N$_4$O$_3$PS$_2$: C, 41.93; H, 4.60; N, 15.04. Found: C, 41.63; H, 4.54; N, 14.88.

6-(Diethylamino)-2-hydroxy-3-(1H-1,2,4-triazol-3-ylamino)-2,3-dihydro-1,2λ⁵-benzoxaphosphol-2-one (4l). Pale yellow solid, yield: 70.4%, mp: 259−261 °C; ^{1}H NMR (400 MHz, DMSO-d_6) δ: 1.24 (t, 6H, 2 × N-CH$_2$CH$_3$), 3.55 (q, 4H, 2 × N-CH$_2$CH$_3$), 3.98 (s, 1H, H-3), 4.24 (s, 1H, H-10), 6.16 (s, 1H, H-7), 6.24 (d, 1H, H-13), 6.92 (d, 1H, H-4), 7.55 (s, 1H, H-14), 13.48 (s, 1H, C$_{14}$-NH) ppm; ^{13}C NMR (100 MHz, DMSO-d_6) δ: 12.6 (2 × N-CH$_2$-CH$_3$), 47.5 (2 × N-CH$_2$-CH$_3$), 74.6 (C-3), 98.4 (C-7), 105.6 (C-5), 119.4 (C-8), 129.5 (C-4), 146.3 (C-14), 149.4 (C-6), 156.8 (C-9), 163.4 (C-11) ppm; ^{31}P NMR (160 MHz, DMSO-d_6) δ: 19.56 ppm. IR (ZnSe) ν (cm^{-1}): 1076 (P−O), 1222 (P=O), 3433 (N−H); ESI MS m/z: 647.8 [2 M + H]$^+$, 324.4 [M + H]$^+$; anal. calcd for C$_{13}$H$_{18}$N$_5$O$_3$P: C, 48.30; H, 5.61; N, 21.66. Found: C, 48.02; H, 5.55; N, 21.53.

Cytotoxicity Assay. Pancreatic cancer cell lines of the study were acquired from the American Type Culture Collection (ATCC, Manassas, VA) and cultured in an RPMI-1370 medium, supplemented with FBS (10%) and penicillin/streptomycin (100 units/mL) at 37 °C. Cells were plated with a starting density of 10^5 cells onto a 96-well plate and treated with title compounds of different concentrations for a period of 48 h, and cell proliferation by MTT assay was measured by taking absorbance at 570 nm by a kinetic microplate reader (BioTek, Winooski, Vermont) on after incubating for a period of 48 h of the logarithmically grown cells.

S Phase Cell Cycle Arrest. Initially, the BxPC-3 cells were subjected for tissue culture and plated on to a 60 × 15 dish with $5 × 10^5$ cells/dish density and allowed to stand overnight. Then, the cells were treated with a test solution of **4a**, **4b**, and **4k** with 50 μM concentration and stand for 48 h and then performed the cell cycle analysis, and FACS (fluorescence activated cell sorter) was used to perform the study. To perform the DNA content analysis, the cells were cultured followed by suspension in 0.5 mL of phosphate buffered saline (PBS) at 4 °C temperature in an ice bath of 70% ethanol and cooled for 2 h. Then, the cells were rehydrated in PBS and then treated with RNase (10 mg/mL) for 30 min, and then the cells were incubated in the dark for 10 min in propidium iodide (10 μg/mL) solution. Cell analysis in a FACS analyzer was performed at 488 nm of excitation wavelength and 585 nm of emission wavelength. Ultimately, the percentage of cells existing in cell cycle was predicted by using Flow Jo (BD biosciences, Rockville, MD) software.

Molecular Docking Studies. The models were prepared by MOE software and predicted the molecular descriptor values. The three-dimensional protein structure of a human ribonucleotide reductase enzyme was granted from the PDB (Protein Data Bank) database[52] and loaded onto the MOE tool and removed the water molecules and other heteroatoms and added the polar hydrogens. Then, the three-dimensional structure was protonated in the solvated environment at 300 K temperature and 7.0 pH and 0.1 salt concentration conditions and then applied the electrostatic potential to the system with 1.5 A° cutoff and 1 unit of dielectric constant values. The Lennard Jones form of van der Waals interactions includes the attractive form of energy at 8 A° of applied cutoff. After the protonation, its complete energy minimized structure was obtained at 0.05 A° of gradient cutoff in AMBER99 force field. Then, the molecular dynamics simulations studies were

performed at 300 K temperature for a duration of 10 ps. The complete simulations were performed for 2000 ps duration with 0.001 of time step and 0.2 ps of temperature relaxation time. The significant parameters like velocity, position, and acceleration were recorded for every 0.5 ps. The three-dimensional energy minimized structures of the interacted ligands were constructed in the MOE working environment. MMFF94x force fields were encompassed, and the related potential energy terms were empowered for all the van der Waals interactions, electrostatic interactions, bonded inter-actions, and restraints with an 8−10 units of enabled cutoff value for the non-bonded interactions. The comprehensive born implicit salvation model was enabled by fixing the other parameters. During the calculation of the parameters, the force field partial charges were enabled and with 0.05 of fixed gradient during the minimization process. The molecular dynamics simulations were performed in the Nosé−Poincaré−Andersen (NPA) formulation algorithm. The initial fixed run time temperature (30 K) was increased to 300 K and 0 ps of heat and cool times.

ADMET Properties. The ADMET properties of compounds **4a-l** like were calculated on the preADMET online server.[53−56] In such, the *in vitro* Caco-2 cell permeability, percentage of human intestinal absorption (% HIA), *in vitro* Madin−Darby Canine Kidney (MDCK) cell permeability, *in vivo* blood−brain barrier (BBB) penetration, and *in vitro* plasma protein binding (PPB) properties were predicted and cognized the ADMET potentialities. Similarly, the toxicity properties like mutagenic, tumorigenic, reproductive, and irritant effects were also predicted. In such, the robust BBB penetrability property of a compound under study helps to decide its ability to be carried in an administered route into the bloodstream and to govern its CNS (central nervous system) activity as such the CNS active compounds have the BBB penetration rate greater than 0.40 and CNS inactive compounds have the BBB penetration rate less than 0.40. Similarly, the Caco-2 cell permeability helps in deciding the capability of Caco-2 cells associating with the intestinal epithelium system in the multiple drug transport pathways like transcellular, paracellular, and active efflux ones. Similarly, the *in vitro* Caco-2 cell permeability helps in deciding a compound's permeability as the permeability value less than 4 indicates that the compounds are poorly permeable, perme-ability value in the range of 4−70 indicates the compounds are moderately permeable, and permeability value greater than 70 indicates the compounds are greatly permeable and hence decides its transportability in cellular and biochemical processes. Likewise, the extent of PPB reveals us the quantity of the unbound compound that is distributed in the body tissues. The percentage of PPB that is greater than 90 indicates the compounds as strongly bound, and the percentage of PPB that is less than 90 indicates the compounds as weakly bound to the tissues and hence denotes its efficacy. In addition, the *in vitro* MDCK permeability categorizes the compounds as poorly permeable if the permeability value is less than 25, and moderately permeable if the value is in the range of 25−500, and greatly permeable if the value is greater than 500 and hence decides their permeable potentiality. Similarly, the percentage of HIA designates the percentage of an orally administered compound in hepatic portal vein and is calculated from the ratio of cumulative excretion in bile, feces, and urine. Ultimately, it decides the analytes as poor absorbing if the value is less than 20, moderately absorbing if the value is in the

range of 20−70, and worthy absorbing if the value is greater than 70 into the human intestine. Similarly, the toxicology study discloses that the negative toxicology of a molecule under examination designates it as prone to carcinogenicity and human ether-a-go-go-related gene (HERG) channel inhibition and mutagenicity and ultimately supports as a safer drug.

QSAR Studies. Drugs under investigation with agreeable ADMET properties will be extended for clinical studies for worthy oral bioavailability as understood from the assurance of their solubility and partitioning properties. It includes the authentication of Lipinski's rule of five[57] in ascertaining the molecule's potentiality such as molecular weight ($\leq$500 da), number of hydrogen bond acceptors ($\leq$10), number of hydrogen bond donors ($\leq$5), logP ($\leq$5, partition coefficient in octanol/water), and molar refractivity (40−130) and hence predicted the Lipinski parameters for **4a−l**. Furthermore, the Veber parameters like total polar surface area and number of rotatable bonds in addition to Lipinski's rule are predicted online with Molinspiration,[58] robust software that helps in computing significant molecular properties of organic com-pounds with structural sensitivity. The additional parameters like solubility, number of hydrophobic atoms, density, van der Waals volume, percentage of absorption, and calculated partition coefficient (octanol to water) have been predicted.[59]

Bioactivity and Toxicity Risk Studies. The QSAR descriptors were evaluated on Molinspiration engine v2018.10, and bioactivity properties were evaluated on Molinspiration engine v2018.03 on the Molinspiration online server.[58] The GPCRL, ICM, KI, and NRL interactions, PI and EI properties, drug-likeness, and drug scores evaluated have evidenced them as safer drugs. Similarly, the drug properties and toxicity risks were predicted online by the Osiris property explorer.[60] In consolidation, it assisted in assessing their physico-chemical interactions of **4a−l** against the selected targets.

■ ASSOCIATED CONTENT

ⓢ Supporting Information

The Supporting Information is available free of charge at https://pubs.acs.org/doi/10.1021/acsomega.1c00360.

> Detailed molecular docking interaction images and InChI codes of compounds **4a−l** (PDF)

■ AUTHOR INFORMATION

Corresponding Authors

Visweswara Rao Pasupuleti − *Department of Biomedical Sciences and Therapeutics, Faculty of Medicine and Health Sciences, Universiti Malaysia Sabah, Kota Kinabalu 88400, Sabah, Malaysia; Department of Biochemistry, Faculty of Medicine and Health Sciences, Abdurrab University, Pekanbaru 28292, Riau, Indonesia*; Email: pvrao@ums.edu.my

Suresh Reddy Cirandur − *Department of Chemistry, Sri Venkateswara University, Tirupati 517 502, India;* ⓞ orcid.org/0000-0002-9804-9683; Email: csrsvu@gmail.com

Authors

Satheesh Krishna Balam − *Department of Chemistry, Sri Venkateswara University, Tirupati 517 502, India*

Jayaprakash Soora Harinath − *Department of Chemistry, Sri Venkateswara University, Tirupati 517 502, India*

Suresh Kumar Krishnammagari − *Department of Chemistry, Sri Venkateswara University, Tirupati 517 502, India*

Raghavendra Reddy Gajjala − *Department of Chemistry, Sri Venkateswara University, Tirupati 517 502, India*

Kishore Polireddy − *Division of Gastroenterology, Hepatology, and Nutrition, Department of Internal Medicine, The University of Texas Health Science Center at Houston, Houston, Texas 77030, United States*

Vijaya Bhaskar Baki − *Department of Pathophysiology, The Key Immunopathology Laboratory of Guangdong Province, Shantou University Medical College, Shantou 515031, Guangdong Province, China*

Wei Gu − *Department of Pathophysiology, The Key Immunopathology Laboratory of Guangdong Province, Shantou University Medical College, Shantou 515031, Guangdong Province, China*

Koteswara Rao Valasani − *Department of Pharmacology & Toxicology and Higuchi Bioscience Center, School of Pharmacy, University of Kansas, Lawrence, Kansas 66047, United States*

Vijaya Kumar Reddy Avula − *Chemical Engineering Institute, Ural Federal University, Yekaterinburg 620002, Russian Federation*

Swetha Vallela − *Chemical Engineering Institute, Ural Federal University, Yekaterinburg 620002, Russian Federation*

Grigory Vasilievich Zyryanov − *Chemical Engineering Institute, Ural Federal University, Yekaterinburg 620002, Russian Federation; Ural Division of the Russian Academy of Sciences, I. Ya. Postovskiy Institute of Organic Synthesis, Yekaterinburg 620219, Russian Federation*

Complete contact information is available at:
https://pubs.acs.org/10.1021/acsomega.1c00360

Notes
The authors declare no competing financial interest.

■ REFERENCES

(1) Mallikarjun Reddy, S.; Reddy, B. N.; Motakatla, V. K. R.; Gokanapalli, A.; Pathak, M.; Reddy, P. V. G. Pd-NHC catalyzed Suzuki-Miyaura couplings on 3-bromo-9H-pyrido[2,3-b]indole-6-sulfonamide. *Synth. Commun.* **2019**, *49*, 1987−1996.

(2) Anusha, G.; Reddy, M. V. K.; Govardhana Reddy, P. V. SingaCycle™-A1-Catalyzed Successive Suzuki-Miyaura and Buchwald Couplings for the Synthesis of Various New Pyridine Analogues. *ChemistrySelect* **2018**, *3*, 13182−13190.

(3) Gokanapalli, A.; Motakatla, V. K.; Peddiahgari, V. G. R. Benzimidazole bearing Pd−PEPPSI complexes catalyzed direct C2-arylation/heteroarylation of N-substituted benzimidazoles. *Appl. Organomet. Chem.* **2020**, *34*, e5869. (1−12).

(4) Naidu, K. R. M.; Rao, P. V.; Raju, C. N.; Srinivasulu, K. Synthesis and Antioxidant Activity of Substituted-1, 3, 2-Diazaphosphole 1-Oxides. *Arch. Pharm.* **2011**, *344*, 765−770.

(5) Rao, A. J.; Rao, P. V.; Rao, V. K.; Mohan, C.; Raju, C. N.; Reddy, C. S. Microwave Assisted One-pot Synthesis of Novel α-Aminophosphonates and heir Biological Activity. *Bull. Korean Chem. Soc.* **2010**, *31*, 1863−1868.

(6) Reddy, S. S.; Rao, V. K.; Krishna, B. S.; Reddy, C. S.; Rao, P. V.; Raju, C. N. Synthesis, antimicrobial, and antioxidant activity of new α-aminophosphonates. *Phosphorus, Sulfur Silicon Relat. Elem.* **2011**, *186*, 1411−1421.

(7) Reddy, O. V. S.; Krishnaiah, M.; Reddy, C. S.; Puranikd, V. G. Synthesis, NMR, X-ray crystallography and bioactivity of some α-aminophosphonates. *ARKIVOC* **2007**, *13*, 133−141.

(8) Prasad, G. S.; Manjunath, M.; Reddy, K. R. K. K.; Reddy, O. V. S.; Reddy, C. S. Synthesis and antibacterial activity of new aryl/alkyl phosphonates *via* Michaelis-Arbuzov rearrangement. *ARKIVOC* **2006**, *16*, 128−135.

(9) Balam, S. K.; Krishnammagari, S. K.; Harinath, J. S.; Sthanikam, S. P.; Chereddy, S. S.; Pasupuleti, V. R.; Yellapu, N. K.; Peddiahgari, V. G. R.; Cirandur, S. R. Synthesis of N-(3-picolyl)-based 1,3,2λ⁵-benzoxazaphosphinamides as potential 11β-HSD1 enzyme inhibitors. *Med. Chem. Res.* **2015**, *24*, 1119−1135.

(10) Yu, Y. C.; Kuang, W. B.; Huang, R. Z.; Fang, Y. L.; Zhang, Y.; Chen, Z. F.; Ma, X. L. Design, synthesis and pharmacological evaluation of new 2-oxo-quinoline derivatives containing α-aminophosphonates as potential antitumor agents. *Med. Chem. Commun.* **2017**, *8*, 1158−1172.

(11) Meyer, J. H.; Bartlett, P. A. Macrocyclic Inhibitors of Penicillopepsin. 1. Design, Synthesis, and Evaluation of an Inhibitor Bridged between P1 and P3. *J. Am. Chem. Soc.* **1998**, *120*, 4600−4609.

(12) Balakrishna, A.; Reddy, C. S.; Naik, S. K.; Manjunath, M.; Raju, C. N. SYNTHESIS, CHARACTERIZATION AND BIO-ACTIVITY OF SOME NEW α-AMINOPHOSPHONATES. *Bull. Chem. Soc. Ethiop.* **2009**, *23*, 69−75.

(13) Smith, B. R.; Eastman, C. M.; Njardarson, J. T. Beyond C, H, O, and N! Analysis of the elemental composition of U.S. FDA approved drug architectures. *J. Med. Chem.* **2014**, *57*, 9764−9773.

(14) Lejczak, B.; Kafarski, P. Biological activity of aminophosphonic acids and their short peptides. In: Bansal, R. (Eds) *Phosphorous heterocycles I. Topics in heterocyclic chemistry*; Vol 20. Springer: Berlin, Heidelberg, 2009, pp. 31−63

(15) Mucha, A.; Kafarski, P.; Berlicki, Ł. Remarkable potential of the α-aminophosphonate/phosphinate structural motif in medicinal chemistry. *J. Med. Chem.* **2011**, *54*, 5955−5980.

(16) Ye, M. Y.; Yao, G. Y.; Pan, Y. M.; Liao, Z. X.; Zhang, Y.; Wang, H. S. Synthesis and antitumor activities of novel α-aminophosphonate derivatives containing an alizarin moiety. *Eur. J. Med. Chem.* **2014**, *83*, 116−128.

(17) Yao, G. Y.; Ye, M. Y.; Huang, R. Z.; Li, Y. J.; Pan, Y. M.; Xu, Q.; Liao, Z. X.; Wang, H. S. Synthesis and antitumor activities of novel rhein α-aminophosphonates conjugates. *Bioorg. Med. Chem. Lett.* **2014**, *24*, 501−507.

(18) Enchev, D. D. Synthesis and biological activity of 2,5-Dihydro-1,2-oxaphosphole-2-oxide derivatives. In: Bansal, R. (Eds) *Phosphorus heterocycles II. Topics in heterocyclic chemistry*; Vol 21. Springer: Berlin, Heidelberg, 2010, pp. 23−62.

(19) Georgieva, A.; Iliev, I.; Topashka-Ancheva, M.; Kraicheva, I.; Tsacheva, I.; Tashev, E.; Tosheva, T.; Kril, A. *In vitro* antitumour activity, safety testing and subcellular distribution of two poly-[oxyethylene(aminophosphonate-co-H-phosphonate)]s in Ehrlich ascites carcinoma and BALB/c 3T3 cell culture systems. *Biotechnol. Biotechnol. Equip.* **2016**, *30*, 192−196.

(20) Fang, Y.-L.; Wu, Z.-L.; Xiao, M.-W.; Tang, Y.-T.; Li, K.-M.; Ye, J.; Xiang, J.-N.; Hu, A.-X.; et al. *Int. J. Mol. Sci.* **2016**, *17*, 653.

(21) Chinthaparthi, R. R.; Bhatnagar, I.; Gangireddy, C. S. R.; Syama, S. C.; Cirandur, S. R. Green synthesis of α-aminophosphonate

derivatives on a solid supported TiO$_2$-SiO$_2$ catalyst and their anticancer activity. *Arch. Pharm.* **2013**, *346*, 667−676.

(22) Prasad, S. S.; Kumar, K. S.; Jayaprakash, S. H.; Krishna, B. S.; Sundar, C. S.; Rao, P. V.; Babu, T. M.; Rajendra, W.; Reddy, C. S. Design, Synthesis, antioxidant, and anti-breast cancer activities of novel diethyl(alkyl/aryl/heteroarylamino)(4-(pyridin-2-yl)phenyl)-methylphosphonates. *Arch. Pharm.* **2013**, *346*, 380−391.

(23) Reddy, C. B.; Kumar, K. S.; Kumar, M. A.; Reddy, M. V. N.; Krishna, B. S.; Naveen, M.; Arunasree, M. K.; Reddy, C. S.; Raju, C. N.; Reddy, C. D. PEG-SO$_3$H catalyzed synthesis and cytotoxicity of α-aminophosphonates. *Eur. J. Med. Chem.* **2012**, *47*, 553−559.

(24) Santhisudha, S.; Madhu Kumar Reddy, K.; Nanda Kumar, Y.; Selvarajan, E.; Mohanasrinivasan, V.; Kumar Nayak, S.; Suresh Reddy, C. Zinc tetrafluoroborate catalyzed synthesis and cytotoxicity of dimethyl((aryl/heteroaryl amino)(4-(pyrrolidin-1-yl)phenyl))-methylphosphonates. *Lett. Drug Des. Discovery* **2017**, *14*, 139−150.

(25) Rao, V. K.; Reddy, S. S.; Krishna, B. S.; Reddy, C. S.; Reddy, N. P.; Reddy, T. C. M.; Raju, C. N.; Ghosh, S. K. Design, synthesis and anti colon cancer activity evaluation of phosphorylated derivatives of lamivudine (3TC). *Lett. Drug Des. Discovery* **2011**, *8*, 59−64.

(26) Drabowicz, J.; Krasowska, D.; Łopusiński, A.; Heugebaert, T. S. A.; Stevens, C. V., Selected five-membered phosphorus heterocycles containing a stereogenic phosphorus. In: Bansal, R. (Eds) *Phosphorus heterocycles II. Topics in heterocyclic chemistry*; Vol *21*. Springer: Berlin, Heidelberg, 2010, pp. 103−147.

(27) Moedritzer, K.; Miller, R. E. Isomeric 1,2-oxaphospholene 2-oxides from the reaction of diacetone alcohol and methyl- or phenylphosphonous dichloride. *J. Org. Chem.* **1982**, *47*, 1530−1534.

(28) Ma, S.; Yu, F.; Zhao, J. Pd(II)-catalyzed coupling-cyclization of 1,2-allenyl phosphonic acid monoesters with allylic halides and their application to the synthesis of 1,3-dihydro[2,1]benzoxaphosphole 1-oxides. *Synlett* **2007**, *2007*, 0583−0586.

(29) Yu, F.; Lian, X.; Ma, S. Pd-catalyzed regio- and stereoselective cyclization−heck reaction of monoesters of 1,2-allenyl phosphonic acids with alkenes. *Org. Lett.* **2007**, *9*, 1703−1706.

(30) Lv, Y.; Hu, G.; Ma, D.; Liu, L. L.; Gao, Y.; Zhao, Y. Palladium-catalyzed domino addition and cyclization of arylboronic acids with 3-hydroxyprop-1-yn-1-yl phosphonates leading to 1,2-oxaspholenes. *J. Org. Chem.* **2015**, *80*, 6908−6914.

(31) Balalaie, S.; Baoosi, L.; Tahoori, F.; Rominger, F.; Bijanzadeh, H. R. Synthesis of functionalized 2,5-dihydro-1,2-oxaphospholes *via* one-pot three-component reaction. *J. Iran. Chem. Soc.* **2015**, *12*, 101−105.

(32) Zhou, Y.; Wang, S.; Chen, C.; Xi, C. Copper-mediated reaction of oxazirconacyclopentenes with dichlorophenylphosphine: a new pathway for the formation of 1,2-oxaphosphole derivatives. *RSC Adv.* **2015**, *5*, 71724−71727.

(33) Xin, N.; Ma, S. Efficient Synthesis of 4-halo-2,5-dihydro-1,2-oxaphosphole 2-oxides from 1,2-allenylphosphonates and CuX$_2$ and subsequent suzuki cross-coupling of the C−Cl bonds. *Eur. J. Org. Chem.* **2012**, *2012*, 3806−3817.

(34) Yavari, I.; Alizadeh, A.; Anary-Abbasinejad, M. Efficient synthesis of functionalized 2,5-dihydro-1,2-oxaphospholes. *Tetrahedron Lett.* **2003**, *44*, 2877−2879.

(35) Prasad, G. S.; Babu, B. H.; Raju, C. N.; Reddy, C. D.; Reddy, C. S. Synthesis of 3-(arylamino)-5-bromo-2-phenyl-2,3-dihydro-2λ^5-benzo[*d*][1,2]-oxaphosphol-2-oxides. *Syn. Commun.* **2009**, *39*, 1310−1316.

(36) Bala Krishna, A.; Suresh Kumar, K.; Ramesh, K.; Suresh Reddy, C.; Nayak, S. K. Synthesis, antibacterial and antioxidant properties of newer 1,2-benzoxaphosphol-2-ones. *Der Pharma Chem.* **2009**, *1*, 40−49.

(37) Wang, B.; Miao, Z.; Huang, Y.; Chen, R. A convenient synthesis of 2-alkoxy-2-oxo-1,4,2-oxazaphosphinanes. *Heteroat. Chem.* **2007**, *18*, 65−69.

(38) Tatarinov, D. A.; Kuznetsov, D. M.; Kostin, A. A.; Mironov, V. F. 2-ethoxy-2,3-dihydro[d][1,2]oxaphosphole 2-oxide in the synthesis of dialkyl(diaryl)(2-hydroxybenzyl)phosphine oxides. *Russ. J. Gen. Chem.* **2016**, *86*, 530−533.

(39) Tatarinov, D. A.; Brel', V. K.; Mironov, V. F. Reaction of 2-chloro-5,5-dimethyl-2,5-dihydro-1,2λ^5-oxaphosphole 2-oxide with organomagnesium compounds. *Russ. J. Org. Chem.* **2015**, *51*, 1245−1248.

(40) Ismailov, I. E.; Ivanov, I. K.; Christov, V. C. Bifunctionalized allenes. Part XV. Synthesis of 2,5-dihydro-1,2-oxaphospholes by electrophilic cyclization reaction of phosphorylated α-hydroxyallenes. *Molecules* **2014**, *19*, 11056−11076.

(41) Jean, N. V.; Remi, G.; Frédéric, B.; Yves, A. B.; Jean, L. P.; David, V. Phosphono- and phosphinolactones in the life sciences, Ch. IV, In *Advances in heterocyclic chemistry*; Eric F. V., Scriven, Christopher A., Ramsden, Eds.; Volume *118*, Academic Press: United Kingdom, 2016, pp. 129−193.

(42) Toghueo, R. M. K.; Kemgne, E. A. M.; Eke, P.; Kanko, M. I. M.; Dize, D.; Sahal, D.; Boyom, F. F. Antiplasmodial potential and GC-MS fingerprint of endophytic fungal extracts derived from *Cameroonian Annona muricata*. *J. Ethnopharmacol.* **2019**, *235*, 111−121.

(43) Solanki, P.; Shekhawat, P. Eco-friendly synthesis and potent antifungal activity of 2-substituted coumaran-3-ones. *Nusantara Biosci.* **2012**, *4*, 101−104.

(44) Wattenberg, L. W.; Lam, L. K.; Fladmoe, A. V. Inhibition of chemical carcinogen-induced neoplasia by coumarins and alpha-angelicalactone. *Cancer Res.* **1979**, *39*, 1651−1654.

(45) Alsaif, G.; Almosnid, N.; Hawkins, I.; Taylor, Z.; Knott, D. L. T.; Handy, S.; Altman, E.; Gao, Y. Evaluation of fourteen aurone derivatives as potential anti-cancer agents. *Curr. Pharm. Biotechnol.* **2017**, *18*, 384−390.

(46) Krečmerová, M.; Pohl, R.; Masojídková, M.; Balzarini, J.; Snoeck, R.; Andrei, G. N(4)-Acyl derivatives as lipophilic prodrugs of cidofovir and its 5-azacytosine analogue, (S)-HPMP-5-azaC: chemistry and antiviral activity. *Bioorg. Med. Chem.* **2014**, *22*, 2896−2906.

(47) Thomas, L.C. *Interpretation of the infrared spectra of organophosphorus compounds*; 1974, Hyden & Sons Ltd: London, New York.

(48) Quin, L.D. *A Guide to organophosphorus chemistry*, 2000, John Wiley & Sons: New York.

(49) Kemp, W, *Organic Spectroscopy*; 1991, 3rd Ed. Palgrave:New York.

(50) Vilar, S.; Cozza, G.; Moro, S. Medicinal chemistry and the molecular operating environment (MOE): Application of QSAR and molecular docking to drug discovery. *Curr. Top. Med. Chem.* **2008**, *8*, 1555−1572.

(51) Vilar, S.; González-Díaz, H.; Santana, L.; Uriarte, E. QSAR model for alignment-free prediction of human breast cancer biomarkers based on electrostatic potentials of protein pseudofolding HP-lattice networks. *J. Comput. Chem.* **2008**, *29*, 2613−2622.

(52) http://www.rcsb.org/pdb

(53) Bakht, M. A.; Yar, M. S.; Abdel-Hamid, S. G.; Al Qasoumi, S. I.; Samad, A. Molecular properties prediction, synthesis and antimicrobial activity of some newer oxadiazole derivatives. *Eur. J. Med. Chem.* **2010**, *45*, 5862−5869.

(54) PreADMET. http://preadmet.bmdrc.org/ (accessed 8th January 2021).

(55) Irvine, J. D.; Takahashi, L.; Lockhart, K.; Cheong, J.; Tolan, J. W.; Selick, H. E.; Grove, J. R. MDCK (Madin-Darby canine kidney) cells: A tool for membrane permeability screening. *J. Pharm. Sci.* **1999**, *88*, 28−33.

(56) Zhao, Y. H.; Le, J.; Abraham, M. H.; Hersey, A.; Eddershaw, P. J.; Luscombe, C. N.; Boutina, D.; Beck, G.; Sherborne, B.; Cooper, I.; Platts, J. A. Evaluation of human intestinal absorption data and subsequent derivation of a quantitative structure-activity relationship (QSAR) with the Abraham descriptors. *J. Pharm. Sci.* **2001**, *90*, 749−784.

(57) Lipinski, C. A.; Lombardo, F.; Dominy, B. W.; Feeney, P. J. Experimental and computational approaches to estimate solubility and permeability in drug discovery and development settings. *Adv. Drug Delivery Rev.* **1997**, *23*, 3−25.

(58) http://www.molinspiration.com/cgi-bin/properties (accessed 16th January 2020).

(59) Yang, C. H.; Hsia, C. W.; Jayakumar, T.; Sheu, J. R.; Hsia, C. H.; Khamrang, T.; Chen, Y. J.; Manubolu, M.; Chang, Y. Structure-activity relationship study of newly synthesized iridium-III complexes as potential series for treating thrombotic diseases. *Int. J. Mol. Sci.* **2018**, *19*, 3641.

(60) *Fragment Based Druglikeness.* https://www.organic-chemistry.org/prog/peo/druglikeness.html (accessed 2nd January 2020).